Monthly Notices
of the
ROYAL ASTRONOMICAL SOCIETY

MNRAS **428,** 3607–3617 (2013) doi:10.1093/mnras/sts304

Swift J045106.8−694803: a highly magnetized neutron star in the Large Magellanic Cloud

H. Klus,[1]★ E. S. Bartlett,[1] A. J. Bird,[1] M. Coe,[1] R. H. D. Corbet[2] and A. Udalski[3]

[1]*The Faculty of Physical and Applied Sciences, University of Southampton, Highfield, Southampton SO17 1BJ*
[2]*X-ray Astrophysics Laboratory, NASA Goddard Space Flight Center, University of Maryland Baltimore County, Mail Code 662, Greenbelt, MD 20771, USA*
[3]*Warsaw University Observatory, Aleje Ujazdowskie 4, 00-478 Warsaw, Poland*

Accepted 2012 October 28. Received 2012 October 19; in original form 2012 September 10

ABSTRACT

We report the analysis of a highly magnetized neutron star in the Large Magellanic Cloud (LMC). The high-mass X-ray binary pulsar Swift J045106.8−694803 has been observed with *Swift* X-ray telescope (XRT) in 2008, the *Rossi X-ray Timing Explorer* (*RXTE*) in 2011 and the *X-ray Multi-Mirror Mission–Newton* (*XMM–Newton*) in 2012. The change in spin period over these four years indicates a spin-up rate of -5.01 ± 0.06 s yr^{-1}, amongst the highest observed for an accreting pulsar. This spin-up rate can be accounted for using Ghosh & Lamb accretion theory assuming it has a magnetic field of $(1.2\pm^{0.2}_{0.7}) \times 10^{14}$ G. This is over the quantum critical field value. There are very few accreting pulsars with such high surface magnetic fields and this is the first of which to be discovered in the LMC. The large spin-up rate is consistent with *Swift* Burst Alert Telescope (BAT) observations which show that Swift J045106.8−694803 has had a consistently high X-ray luminosity for at least five years. Optical spectra have been used to classify the optical counterpart of Swift J045106.8−694803 as a B0-1 III-V star and a possible orbital period of 21.631 ± 0.005 d has been found from Massive Compact Halo Object (MACHO) optical photometry.

Key words: stars: magnetars – stars: neutron – X-rays: binaries.

1 INTRODUCTION

High-mass X-ray binaries (HMXB) are binary systems composed of either a neutron star, white dwarf or black hole and an optical companion, either a supergiant star – in the case of supergiant X-ray binaries – or a dwarf, subgiant or giant OBe star – in the case of Be/X-ray binaries (BeXB). HMXB can be detected by the X-ray, optical and infrared emission they produce.

X-rays are produced as matter is transferred from the optical star to its denser companion. It is accelerated as it moves into the gravitational potential well produced by the denser star and – if the denser star is a neutron star – it is then channelled by the star's magnetic field lines to the magnetic poles. The accreted matter then rapidly decelerates when it reaches the surface and potential energy is converted to heat which energizes the plasma, producing X-ray hot spots. These can appear as 'beams' if they periodically travel past our line of sight as the star rotates. The pulsation period is equated with the rotation period of the neutron star's crust and this value changes with time as accreted matter transfers angular momentum to or from the star.

HMXB are composed of massive, and therefore relatively short lived, stars and so their presence indicates that a new population of stars formed relatively recently (Grimm, Gilfanov & Sunyaev 2003). This may be the reason why more HMXB have been discovered in the Milky Way and the Small Magellanic Cloud (SMC) than the Large Magellanic Cloud (LMC).

The HMXB in the Milky Way are mostly found within the spiral arms (Coleiro & Chaty 2011) and the SMC underwent a burst of star formation about 200 Myr ago when it was about three times closer to the LMC than it is today (Gardiner & Noguchi 1996; McBride et al. 2010). The SMC has an HMXB population which is comparable in number to the Galaxy despite being almost two hundred times less massive. Whilst about half of the HMXB in the Galaxy are BeXB, all but one HMXB in the SMC is a BeXB system. The LMC, on the other hand, contains relatively few HMXB, most of which are BeXBs (Negueruela & Coe 2002; Liu, van Paradijs & van den Hauvel 2005; Sturm et al. 2012).

Swift J045106.8−694803 is part of a newly discovered BeXB system located in the LMC. It was first discovered by Beardmore et al. (2009) at an RA, Dec. (J2000) of 04:51:06.8 and −69:48:03.2, respectively, with an uncertainty of 3.5 arcsec. Beardmore et al. measured an X-ray flux of $(1.68 \pm 0.11) \times 10^{-11}$ erg cm^{-2} s^{-1} over 0.3–10 keV, fitted with a power law of photon index $0.96\pm^{0.06}_{0.04}$ with a column density of $(1.9 \pm 0.3) \times 10^{21}$ cm^{-2}.

★ E-mail: hvk1g11@soton.ac.uk

Table 1. Summary of XRT data sets.

Observation ID	Start date	Start time	Exposure (ks)
00038029001	2008-10-23	03:56:38	6.56
00038029002	2008-11-11	14:35:46	6.40
00038029003	2008-11-14	00:18:15	2.59
00038029004	2009-01-10	13:23:59	4.32
00038029005	2011-09-30	16:50:35	4.47
00038029006	2011-10-03	18:28:46	5.90

The 14–195 keV flux was found to be $(2.8 \pm 0.3) \times 10^{-11}$ erg cm^{-2} s^{-1} fitted with a power law of photon index 2.5 ± 0.4. Beardmore et al. also report a pulsation period of 187 s. The optical companion to this X-ray source is the $V = 14.70$ blue star [M2002] 9775 (Massey 2002) with an orbital period of 21.64 ± 0.02 d.

Grebenev et al. have recently calculated a photon index of 0.5 ± 0.5 using data from *INTEGRAL*. They have also created energy spectra over 3–200 keV showing that the energy of the high-energy cut-off in the spectrum is at 16.0 ± 5.0 keV (Grebenev et al. 2012).

In this paper, we look at Swift J045106.8−694803 in more detail, confirming its luminosity, pulse period, orbital period and spin-up rate which can be used to determine the strength of its magnetic field.

2 OBSERVATIONS

2.1 X-ray Observations

2.1.1 *Swift/XRT*

Swift's X-ray Telescope (XRT) is a CCD imaging spectrometer operating over 0.2–10 keV in photon counting mode. Archival data were taken from NASA's High Energy Astrophysics Science Archive Research Center (HEASARC)[1] covering six time periods from 2008 October 23 to 2011 October 3, as summarized in Table 1.

The images were extracted using the FTOOL[2] XSELECT. Source and background spectra were then extracted from regions of 34 arcsec radii. The spectra were binned to have 50 counts bin^{-1}. The ancillary response files (ARF) were calculated with XRTMKARF and a redistribution matrix file (RMF) was taken from HEASARC's calibration data base (CALDB). The position of the source was confirmed using FTOOL XRTCENTROID.

The total count rate and error of each data set, as well as the intrinsic H I column density (N_H) and photon index, were calculated using FTOOL XSPEC. The spectra were described by an absorbed power law with a fixed Galactic foreground column density of 8.4×10^{20} cm^{-2} (Dickey & Lockman 1990) and abundances set in accordance with Wilms, Allen & McCray (2000). Intrinsic absorption and the abundances of elements heavier than helium were set to 0.4 (Borkowski, Hendrick & Reynolds 2006). X-ray spectra were then compiled in XSPEC over 0.2–10 keV.

The 0.2–10 keV flux of each data set was determined using XSPEC. The luminosity was then calculated using a distance of 50.6 ± 1.6 kpc (Bonanos et al. 2011).

The light curve of each data set was extracted in XSELECT and a Lomb–Scargle normalized periodogram was produced for each using time series analysis package PERIOD.[3]

[1] http://heasarc.gsfc.nasa.gov/

[2] http://heasarc.nasa.gov/ftools/

[3] http://www.starlink.rl.ac.uk/docs/sun167.htx/sun167.html

Table 2. Summary of *RXTE* data sets.

Observation ID	Start date	Start time	Exposure (ks)
96441-01-01-00	2011-10-28	13:54:55.6	9.005
96441-01-01-01	2011-10-28	10:51:38.6	0.849

2.1.2 *Swift/BAT*

The *Swift* Burst Alert Telescope (BAT) data were taken with the Hard X-ray Transient Monitor from 2004 December 16 to the 2010 May 31 over 14–195 keV. A 58 month light curve was downloaded from NASA's *Swift*/BAT 58-Month Hard X-ray Survey.[4] This contained an average of ∼15 observations a day split into eight energy bands.

2.1.3 *RXTE*

Archival data were taken from HEASARC. These were recorded in two data sets on the 2011 October 28 using the *Rossi X-ray Timing Explorer* (*RXTE*) Proportional Counter Array, over ∼3–10 keV, as summarized in Table 2.

Cleaned light curves were produced for each data set and combined. A Lomb–Scargle normalized periodogram was then created using a frequency interval of 1×10^{-5} Hz.

2.2 Optical observations

2.2.1 *Optical photometry*

Archival data were taken from the Massive Compact Halo Objects (MACHO) project using the 1.27 m telescope at the Mount Stromlo Observatory in Australia. This covered the period from 1992 November 1 to 1999 December 29 and contained instrumental magnitudes using red (*R*) and blue (*B*) filters.

The data were filtered to remove results flagged as erroneous. The four points remaining in the *R*-band data set which were over 2.4 standard deviations from the mean were also removed. This left 96 data points in the red and 207 in the blue. A Lomb–Scargle normalized periodogram was then created in PERIOD for both the *R*- and *B*-band data sets using a frequency interval of 1×10^{-5} Hz and detrending using a polynomial of order 3.

2.2.2 *Optical spectroscopy*

Optical spectra of Swift J045106.8−694803 have been taken on three separate occasions. Red-end spectra were taken with the 1.9 m Radcliffe telescope at the South African Astronomical Observatory (SAAO) on 2009 December 12 and 2011 September 26. The data were obtained using the unit spectrograph combined with a 1200 lines mm^{-1} grating and the Scientific Imaging Technologies, Inc (SITe) detector at the Cassegrain focus. The resulting spectra have a spectral resolution of ∼3 Å. Comparison copper–neon spectra were taken immediately before and after the observation and were used for wavelength calibration.

The source was also observed on 2011 December 8 and 10 with the New Technology Telescope (NTT), La Silla, Chile. Grisms 14 and 20 on the ESO Faint Object Spectrograph (EFOSC2) were used for blue- and red-end spectroscopy, respectively, with a slit width of 1.5 arcsec. Grism 14 has a grating of 600 lines mm^{-1} that yielded

[4] http://swift.gsfc.nasa.gov/docs/swift/results/bs58mon/

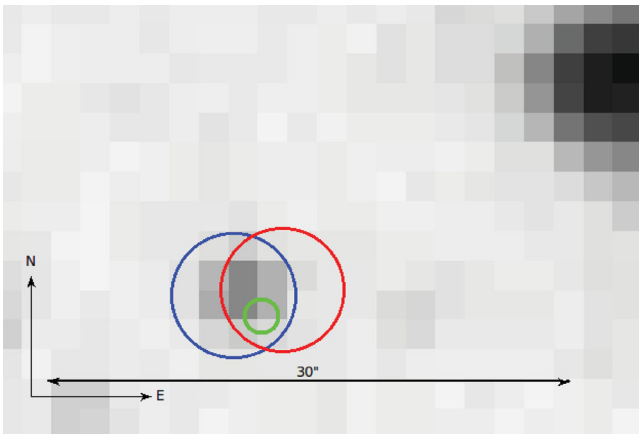

Figure 1. Uncertainty circles of the X-ray source overlaid on an optical background (from ESO DSS II Blue). The red circle shows the position found using the *Swift*/XRT data set 00038029001, the blue circle using data set 00038029002 and the green using the *XMM–Newton* data set from Bartlett et al. (in preparation).

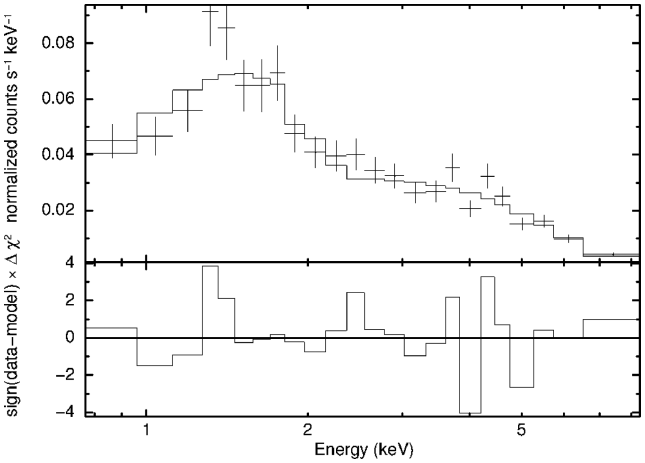

Figure 2. The upper panel shows the X-ray spectrum from *Swift*/XRT data set 00038029001 over 0.2–10 keV, here the photon index is 0.7 ± 0.1 with a N_H of 3 ± 2 counts/s, the lower panel shows residuals.

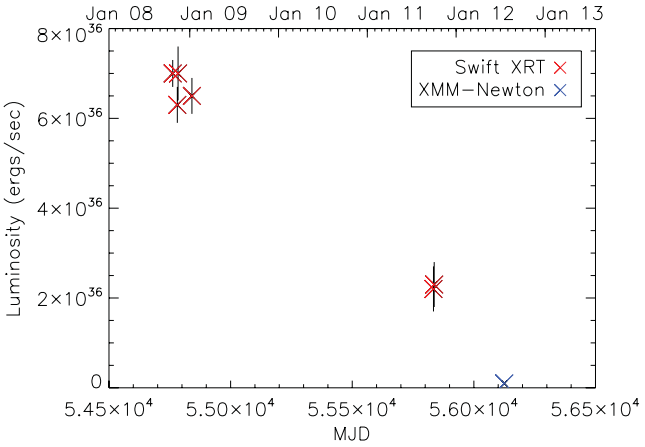

Figure 3. Luminosity plotted against time for the *Swift*/XRT and *XMM–Newton* data sets over 0.2–10 keV. *XMM–Newton* data set is from Bartlett et al. (in preparation).

1 Å pixel^{-1} dispersion over a wavelength range of λλ3095–5085 Å. Grism 20 is one of the two new Volume-Phase Holographic grisms recently added to EFOSC2. It has a smaller wavelength range, from 6047–7147 Å, but a superior dispersion of 0.55 Å pixel^{-1} and 1070 lines pixel^{-1}. Filter OG530 was used to block second-order effects. The resulting spectra were recorded on a Loral/Lesser, thinned, AR-coated, UV flooded, MPP CCD with 2048 × 2048 pixels, at a spectral resolution of ∼10 and ∼6 Å, respectively. Wavelength calibration was achieved using comparison spectra of helium and argon lamps taken through out the observing run with the same instrument configuration.

The data were reduced using the standard packages available in the Image Reduction and Analysis Facility (IRAF). The resulting spectra were normalized to remove the continuum and a redshift correction applied corresponding to the recession velocity of the LMC, taken as −280 km s^{-1} (Paturel et al. 2002).

3 RESULTS

3.1 X-ray Results

3.1.1 Swift/XRT

Fig. 1 shows the positions calculated for data sets 00038029001 (red) and 00038029002 (blue). The first data set has an RA, Dec (J2000) of 04:51:06.4 and −69:48:02.5 with a 2σ error radius of 3.6 arcsec. The second has an RA, Dec. (J2000) of 04:51:07.0 and −69:48:03.1 with a 2σ error radius of 3.6 arcsec. These are consistent with the positions calculated by Beardmore et al. (2009).

The results of data extracted using XSPEC are summarized in Table 3. Fig. 2 shows the X-ray spectra of data set 00038029001 over 0.2–10 keV. This shows that the counts can be divided equally into four energy ranges of 0.5–1.5, 1.5–3, 3–4.5 and 4.5–8 keV. The X-ray luminosities are plotted in Fig. 3, which shows that the X-ray luminosities measured between 2008 October and 2009 January

Table 3. Summary of the information extracted from the spectra of *Swift*/XRT data sets 00038029001–00038029006 over 0.2–10 keV using a distance of 50.6 ± 1.6 kpc (Bonanos et al. 2011).

	Observation ID	Count rate (counts s^{-1}) over 0.2–10 keV	N_H (10^{21} cm^{-2})	Photon index	Flux (10^{-11} erg s^{-1} cm^{-2})	Luminosity (10^{36} erg s^{-1})	Reduced χ^2	Degree of freedom
a	00038029001	0.198 ± 0.006	3 ± 2	0.7 ± 0.1	2.3 ± 0.1	7.0 ± 0.3	1.4	21
b	00038029002	0.175 ± 0.005	1 ± 2	0.7 ± 0.1	2.1 ± 0.1	6.3 ± 0.4	1.2	17
c	00038029003	0.182 ± 0.008	3 ± 7	0.6 ± 0.2	2.3 ± 0.2	7.0 ± 0.6	0.6	5
d	00038029004	0.181 ± 0.006	1 ± 3	0.6 ± 0.1	2.1 ± 0.1	6.5 ± 0.4	1.2	11
e	00038029005	0.073 ± 0.004	15 ± 14	1.1 ± 0.4	0.7 ± 0.2	2.2 ± 0.5	0.8	2
f	00038029006	0.058 ± 0.003	1 ± 16	0.6 ± 0.4	0.8 ± 0.2	2.3 ± 0.5	2.0	2

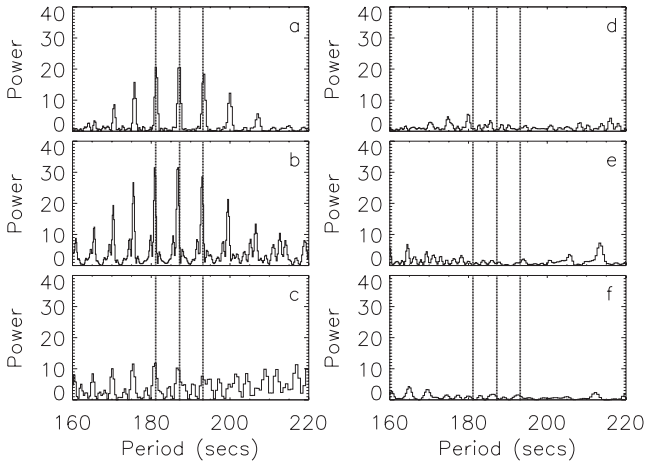

Figure 4. Lomb–Scargle normalized periodograms for *Swift*/XRT data sets 00038029001–00038029006 (labelled a–f) over 0.2–10 keV. The dotted lines indicate the 187 s period and the two side peaks of 181 and 193 s mentioned by Beardmore et al. (2009).

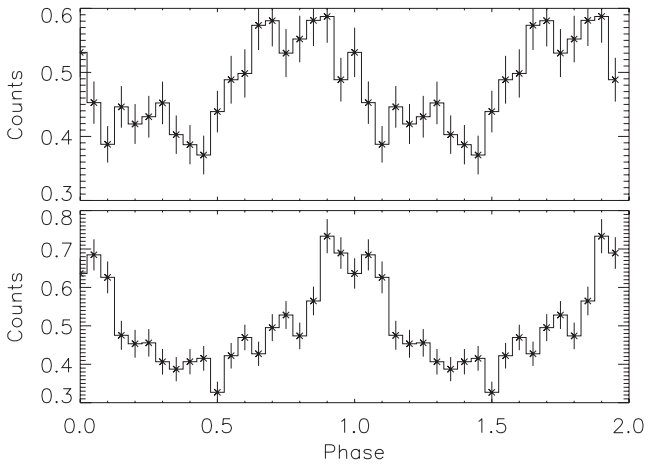

Figure 5. Light curves from *Swift*/XRT data sets 00038029001 (top panel) and 00038029002 (bottom panel) over 0.2–10 keV, folded at 187.0 and 186.8 s, respectively. The phase shift is arbitrary.

were about four times higher than those measured in 2011 October and September.

Fig. 4 shows the Lomb–Scargle normalized periodogram for each of the six data sets. A period is only evident in data sets 00038029001 and 00038029002, these are 187.0 ± 0.3 and 186.8 ± 0.2 s, respectively, and show no harmonics. This indicates that light curves folded at these values should be sinusoidal. Folded light curves for data sets 00038029001 and 00038029002 are shown in Fig. 5.

Light curves for data set 00038029001 in each of the four energy ranges determined from Fig. 2 are shown in Fig. 6. A plot of pulse-fraction against energy is shown in Fig. 7. The pulse-fraction appears to increase with increasing energy between 0.5 and 4.5 keV and then decrease; however, the large error bars make this inconclusive.

The side peaks in the periodograms are due to gaps in the observations. This was confirmed first by fitting a sine wave with the same period to the data, which gave rise to identical peaks, and secondly, by splitting data set 00038029001 into six shorter data sets

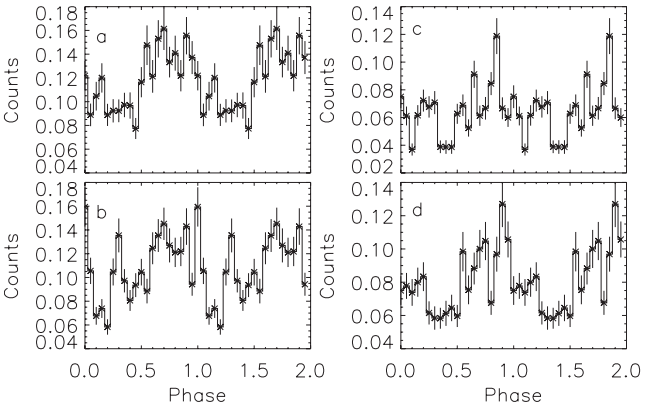

Figure 6. Light curves from *Swift*/XRT data set 00038029001, folded at 187.0 s, over 0.5–1.5, 1.5–3, 3–4.5 and 4.5–8 keV (labelled a–d).

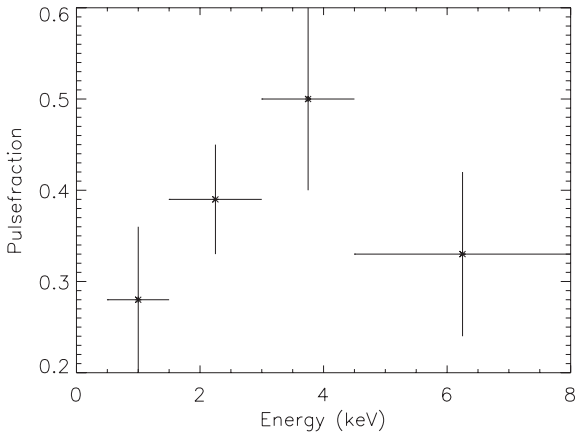

Figure 7. Pulse-fraction plotted against energy for *Swift*/XRT data set 00038029001 folded at 187.0 s, over 0.5–1.5, 1.5–3, 3–4.5 and 4.5–8 keV.

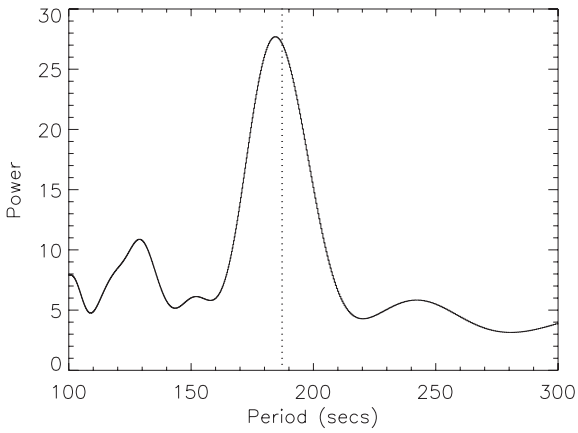

Figure 8. Lomb–Scargle normalized periodogram created by splitting data set 00038029001 into six data sets composed of continuous observations and adding the periodograms. The dotted line indicates the 187.0 s period found for data set 00038029001.

composed of continuous observations and adding the individual periodograms, as can be seen in Fig. 8.

Data sets 00038029001 and 00038029002 provided the best signal and so their light curves were combined to determine the best estimation for the pulse period in late 2008. A Lomb–Scargle normalized periodogram yielded a maximum peak at 186.85 ± 0.04 s

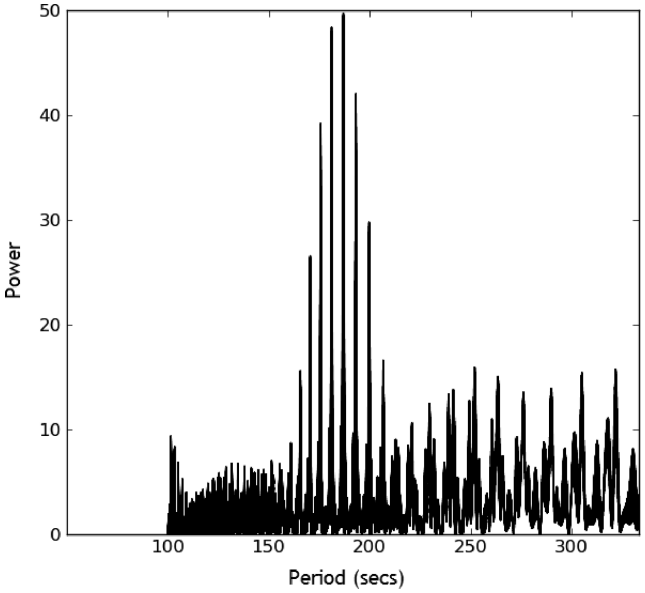

Figure 9. Lomb–Scargle normalized periodogram from *Swift*/XRT data sets 00038029001 and 00038029002 over 0.2–10 keV showing a maximum peak at 186.85 ± 0.04 s. The side peaks are due to gaps in the observations.

as can be seen in Fig. 9. Monte Carlo simulations give this period a 99.9 per cent confidence level. Bootstrapping was conducted in order to confirm that this is the correct peak, and not a product of the window function, and after 5000 iterations between 166 and 200 s, a period of 187.07 ± 0.04 s was found 63 per cent of the time and 181.41 ± 0.04 s was found 37 per cent of the time. We therefore concluded that 187.07 ± 0.04 s was the most probable period of Swift J045106.8−694803 in 2008 October/November.

3.1.2 *Swift/BAT and INTEGRAL/IBIS*

The top panel of Fig. 10 shows the long-term light curve of Swift J045106.8−694803 with total counts over 14–195 keV, binned at 28 d. The count rate appears to increase over time, peaking in about 2007 July and continuing to remain above zero for the next three years.

This was confirmed by the light curve compiled from the *INTEGRAL* IBIS data which is shown in the second panel of Fig. 10. The bottom panel shows the light curve of the optical counterpart taken from Optical Gravitational Lensing Experiment (OGLE) III and IV in the *I* band. The OGLE data shows that the source was brightest in the *I* band whilst it was barely detectable in the X-ray. There is a slight increase in brightness after MJD 54000 but this is not significant.

A Lomb–Scargle normalized periodogram was created for the BAT data set using PERIOD with a frequency interval of 1×10^{-5} Hz but no periods were detected.

3.1.3 *RXTE*

The Lomb–Scargle normalized periodogram is shown in plots (a) and (b) of Fig. 11. As with the *Swift*/XRT data, the side peaks are due to gaps in the observations. This was confirmed by fitting a sine wave with the same period to the data, as can be seen in plot (c) of Fig. 11. The harmonics at exactly 1/3 and 1/4 of the pulse period, seen in the plot (a), indicate that the light curve should be

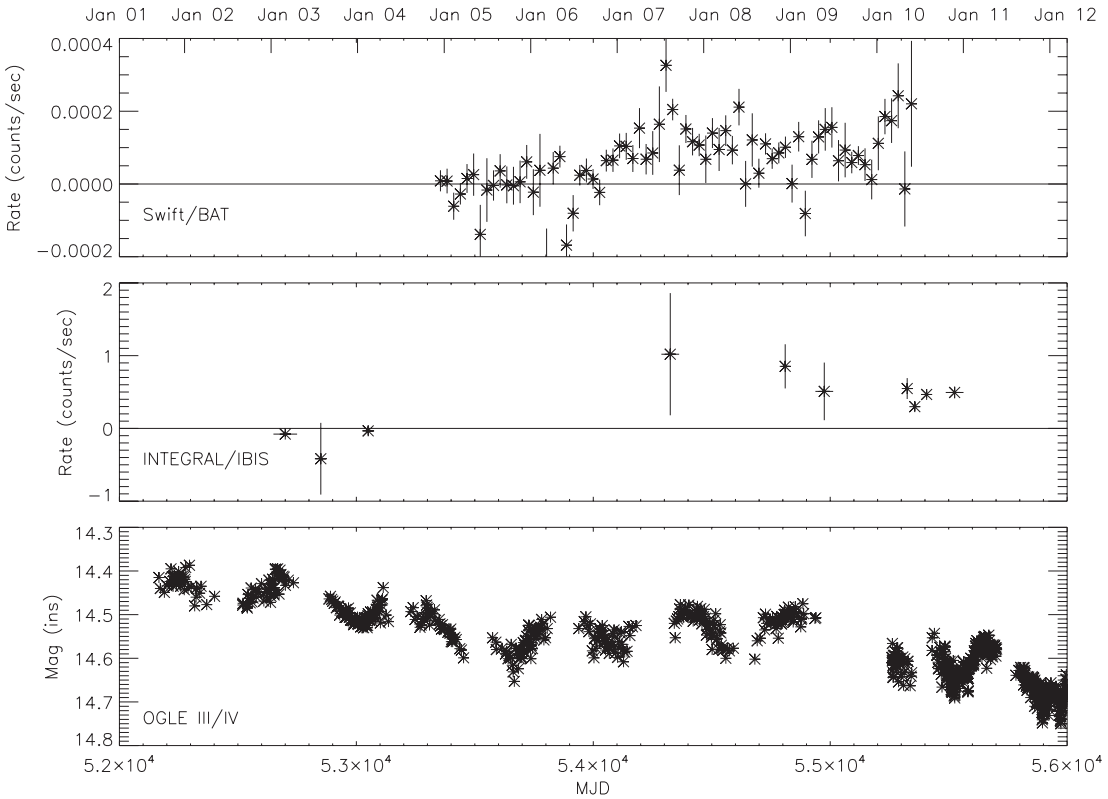

Figure 10. Long-term light curve from *Swift*/BAT (14–195 keV), *INTEGRAL* IBIS (15 keV to 10 MeV) and OGLE III and IV.

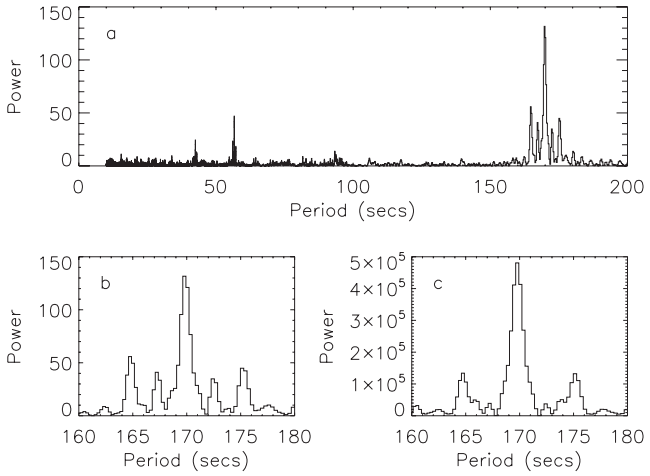

Figure 11. Panel (a) shows the Lomb–Scargle normalized periodogram from the combined *RXTE* data sets over 3–10 keV. Panel (b) shows a close-up view of the region around the main peak compared to panel (c) which shows the result of a simulated data set produced by a pure sine wave of period 169.78 s.

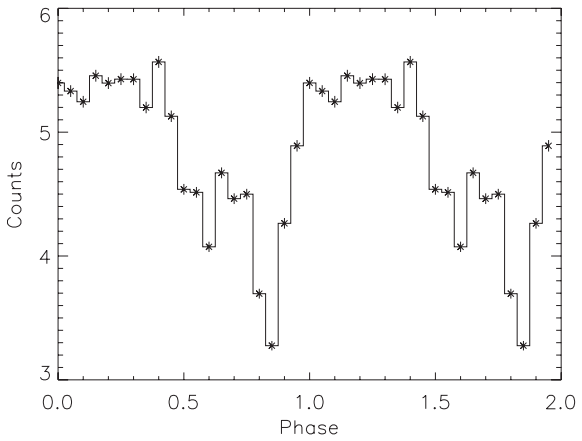

Figure 12. Light curve folded at 169.78 s from *RXTE* data sets 96441-01-01-00 and 96441-01-01-01 over 3–10 keV.

non-sinusoidal and have multiple peaks when folded at the pulse period, as shown in Fig. 12.

The shape of the light curve contains information on the emission geometry from the regions close to the neutron stars magnetic poles. At high luminosities photons can escape from the sides of the accretion column, giving rise to a fan-beam pattern and a more complex profile than that found at lower luminosities where X-rays are generally emitted in a pencil-beam.

The *RXTE* data show a pulsation period of 169.8 ± 0.3 s, 17.3 ± 0.3 s less than the period evident in the *Swift*/XRT data sets taken in 2008 October and November. This gives a spin-up rate ($\dot{P}$) of -5.8 ± 0.1 s yr^{-1}, or $(-1.84 \pm 0.03) \times 10^{-7}$ s s^{-1}, and a spin-up time-scale (T_s) of -30.8 ± 0.5 yr using

$$T_s = \frac{P}{-\dot{P}}, \quad (1)$$

where P is the average pulse period in seconds. Since this is an average over three years, it is possible that the spin-up rate has been much higher at points during this period.

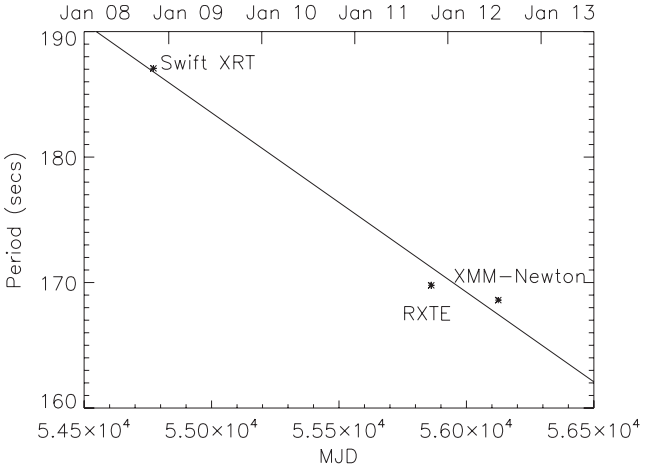

Figure 13. Plot showing the three periods measured by *Swift*/XRT in 2008, *RXTE* in 2011 and *XMM–Newton* in 2012 (Bartlett et al., in preparation). The straight line is a line of best fit showing that the period is continuing to decrease, despite the fact that the rate of change is also decreasing.

3.1.4 XMM–Newton

Swift J045106.8−694803 was observed by the *X-ray Multi-Mirror Mission–Newton* (*XMM–Newton*) on 2012 July 17 (Bartlett et al., in preparation). This confirmed the position of Swift J045106.8−694803 – as shown in Fig. 1 – and gave an up-to-date period and luminosity. The position was found to be at an RA, Dec. (J2000) of 04:51:06.7 and −69:48:04.2, respectively, with a 1σ uncertainty of 1 arcsec. The luminosity was found to be $(9.8 \pm 0.9) \times 10^{34}$ erg s^{-1} – as shown in Fig. 3 – and the period 168.5 ± 0.2 s.

This is 1.3 ± 0.4 s less than the period calculated from *RXTE* in 2011, giving a $\dot{P}$ of -1.8 ± 0.5 s yr^{-1}. It is also 18.6 ± 0.2 s less than the period calculated from *Swift*/XRT in 2008, giving an average $\dot{P}$ of -5.01 ± 0.06 s yr^{-1} and a T_s of -34.9 ± 0.4 yr. Fig. 13 shows the three periods measured by *Swift*/XRT in 2008, *RXTE* in 2011 and *XMM–Newton* in 2012. The luminosity and rate of change of spin period may be decreasing but Swift J045106.8−694803 is still continuing to spin up at a high rate.

3.2 Optical results

3.2.1 Optical photometry

Fig. 14 shows that the flux of the optical companion to Swift J045106.8−694803 appears to have remained fairly consistent in the *B* and *R* bands over 7 yr. The *B*-band data set shows a possible orbital period of 21.631 ± 0.005 d as seen in Fig. 15, although any underlying non-radial pulsations from the Be star may affect the results (Bird et al. 2012). Non-radial pulsations occur when some parts of the stellar surface move inwards while others move outwards at the same time. It has been suggested that they could help form the Be stars circumstellar disc. If the rotational velocity of the Be star is close to the critical velocity, then pulsations lead to matter being ejected and spun up to form a Keplerian disc (Reig 2011).

This period is not evident in the *R* band, this is most likely due to the lack of data points rather than the consequence of a real effect. This idea was confirmed by randomly removing half of the *B*-band data points and creating a new Lomb–Scargle normalized periodogram, which also failed to show any evidence of an orbital period. A light curve folded at 21.631 d was then produced for

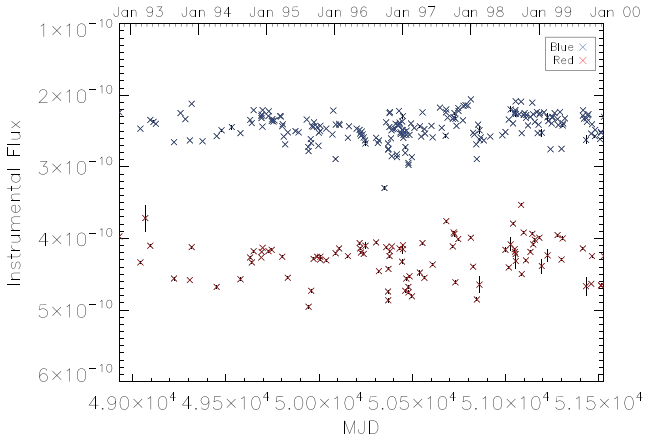

Figure 14. Light curves for the *R*- and *B*-band MACHO data sets.

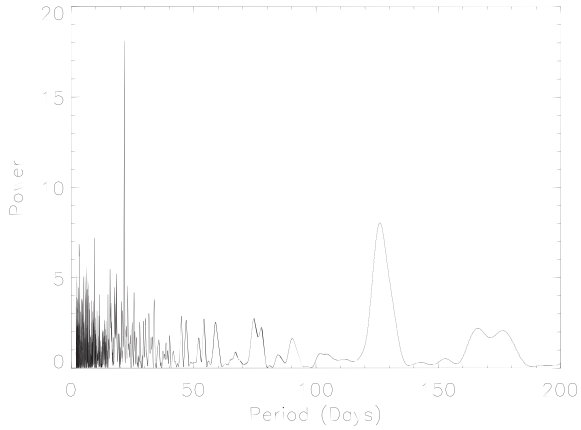

Figure 15. Lomb–Scargle normalized periodogram for the *B*-band MACHO data set showing a possible orbital period of 21.631 ± 0.005 d.

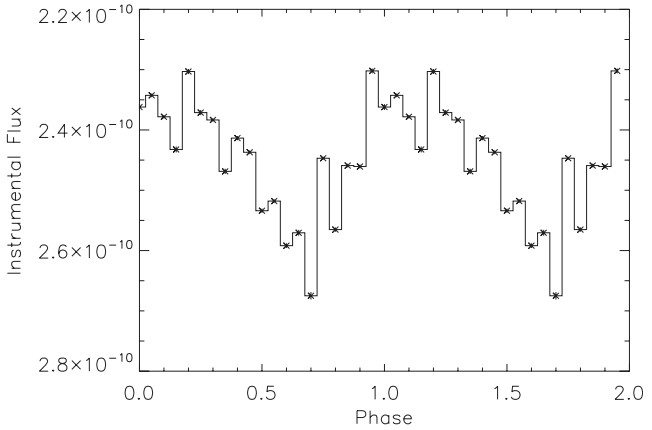

Figure 16. Light curve from the *B*-band MACHO data set folded at 21.631 d.

the *B*-band data set as shown in Fig. 16. Colour ratio and colour magnitude diagrams were also produced. These confirmed that the magnitude in each colour band has remained fairly consistent over the observation period.

Swift J045106.8−694803 was also observed as part of the OGLE III (LMC136.6.14874) and OGLE IV (LMC531.05.4251) programmes. These *I*-band data cover, in total, a duration of more than a decade, and are shown in the bottom panel of Fig. 10. From this figure it is clear that the source undergoes a significant long-term modulation on periods in excess of 400 d. Formally, a Lomb–Scargle power spectrum gives the peak to be around 440 d, but a visual inspection of the light curve shows that there are other time-scale changes occurring. It is therefore unlikely that this long period is related directly to the binary period, but rather may either indicate a general time-scale for fluctuations in the stellar wind, or precessional motion of the circumstellar disc. All these variations make it very difficult to search for confirmation of the 21.631 d period seen in the MACHO data. However, if only the better-sampled OGLE IV data are merged with the MACHO data (normalized to the approximate starting magnitude of the OGLE III data), then the strength of the 21.631 d peak in the Lomb–Scargle power spectrum increases slightly. But without the prior knowledge of this period from the MACHO data such a period would not have been found in the OGLE data.

3.2.2 Optical spectroscopy

OB stars in the Milky Way are classified using certain metal and helium line ratios (Walborn & Fitzpatrick 1990) based on the Morgan–Keenan system (MK; Morgan, Keenan & Kellman 1943). However, this is unsuitable in lower metallicity environments as the metal lines are either much weaker or not present. As such, the optical spectrum of IGR J05414−6858 was classified using the method developed by Lennon (1997) for B-type stars in the SMC and implemented for the SMC, LMC and Galaxy by Evans et al. (2004, 2007).

Fig. 17 shows the unsmoothed optical spectrum of Swift J045106.8−694803. The spectrum is dominated by the hydrogen Balmer series and neutral helium lines. There does appear to be evidence for the He II λ4200 Å line, but it is difficult to distinguish above the noise level along with the He II λλ4541, 4686 Å lines. The He I λ4143 Å line is clearly stronger than the He II λ4200 Å line constraining the optical counterpart of Swift J045106.8−694803 to be later than type O9. There also appears to be evidence for the Si IV λ4088, λ4116 Å lines necessary for a B1 classification. This is supported by the relative strengths of the Si III λ4553 Å and Mg II λ4481 Å suggesting a classification of B2 or earlier.

The luminosity class of the companion star was determined by the ratios of S IV λ4088/He Iλλ4026 − 4121 Å, S IV λ4116/He I λ4121 and He II λ4686/He I λ4713. The first two ratios strengthen with decreasing luminosity class (i.e. with increasing luminosity) whereas the latter ratio decreases with increasing luminosity. The relative strengths of these lines are contradictory. The He II λ4686/He I λ4713 and S IV λ4116/He I λ4121 ratios suggest a luminosity class III, although the proximity of the rotationally broadened Hδ λ4102 Å to the Si IV lines makes this more complex. The S IV λ4088/He I λ4026 ratio is more consistent with a star of luminosity class V. The *V*-band magnitude of this star is reported by several sources as between 14.6 and 14.7 (e.g. Massey 2002; Zaritsky et al. 2004). An M_V of -4.3 ± 0.1 was calculated using a distance modulus of 18.52 ± 0.07 (Bonanos et al. 2011) along with an m_V of 14.65 ± 0.05 and an extinction $A_V = 0.4 \pm 0.1$ (calculated using the Galactic column density towards the source, $8.4 \pm 1.0 \times 10^{20}$ cm^{-2} and the results of Güver & Özel 2009). This is consistent with B0.5III (Wegner 2006). Less information is available for the absolute magnitude of emission line stars, which will be dependent on the inclination and size of the disc. As such we classify the optical counterpart of Swift J045106.8−694803 as a B0-1 III-V star.

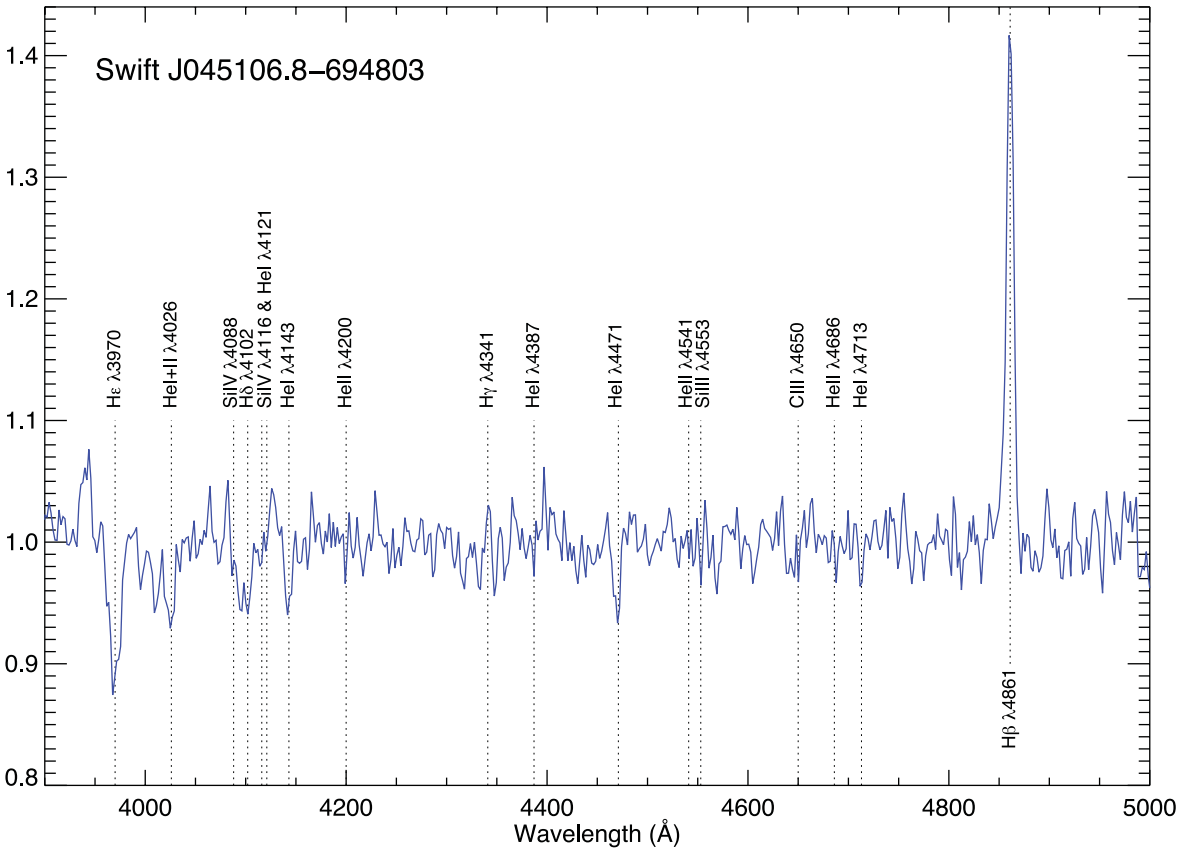

Figure 17. Spectrum of Swift J045106.8−694803 in the wavelength range λλ3900–5000 Å with the NTT on 2011 December 8. The spectrum has been normalized to remove the continuum and redshift corrected by −280 km s^{-1}. Atomic transitions relevant to spectral classification have been marked.

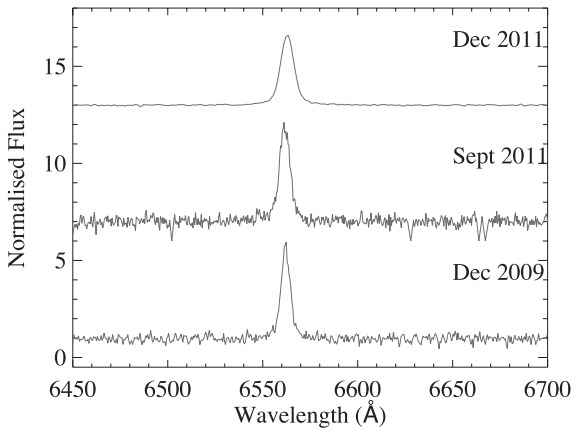

Figure 18. ESO (top panel) and SAAO (middle and bottom panels) spectra of Swift J045106.8−694803 in the wavelength range λλ6400–6700 Å with the NTT on 2011 December 10. Spectra have been normalized to remove the continuum and shifted by −280 km s^{-1}.

Fig. 18 shows the three red-end spectra of Swift J045106.8−694803 taken two years apart. The ESO (top) spectrum is offset by six flux units. The Hα equivalent width, considered an indicator for circumstellar disc size, is remarkably similar in all three spectra increasing from -29 ± 2 Å for the SAAO spectrum taken in 2009 to -33 ± 1 and -34.5 ± 0.6 Å for the SAAO and ESO spectra taken in 2011. It is not uncommon to see large variations in the Hα equivalent width of these systems on time-scales of months. This apparent consistency in the equivalent width (and hence the disc size) is almost certainly linked to the exceptionally persistent X-ray activity of the source.

4 DISCUSSION AND CONCLUSIONS

We have confirmed the pulsation and orbital periods given by Beardmore et al. (2009). Recent measurements show that Swift J045106.8−694803 has spun up at a rate of ∼5 s yr^{-1} for the last four years and although this rate is decreasing with luminosity, it is still continuing to spin up at a high rate.

Swift J045106.8−694803 may have experienced one of the highest spin-up rates of any known accreting pulsar but this can be accounted for using Ghosh & Lamb (1979) accretion theory assuming that the stellar magnetic field is dipolar and that it is accreting from a Keplerian disc.

Accretion theory shows that the magnetic field (B) of a disc-fed accreting pulsar is related to the rate of change of its spin period ($\dot{P}$), its average spin period (P) and its average luminosity (L).

In general, the higher the mass accretion rate ($\dot{M}$), the higher the luminosity and the more angular momentum is accreted per second. Where magnetic stresses dominate matter flow at surface S1 – as seen in Fig. 19 from Ghosh & Lamb (1979) – this almost always causes spin-up.

At surface S2, where viscous stresses dominate, this can add a spin-up or spin-down torque depending on the stars fastness parameter (ω_s). This is the ratio between the angular velocity of the neutron star and the Keplerian angular velocity of the disc.

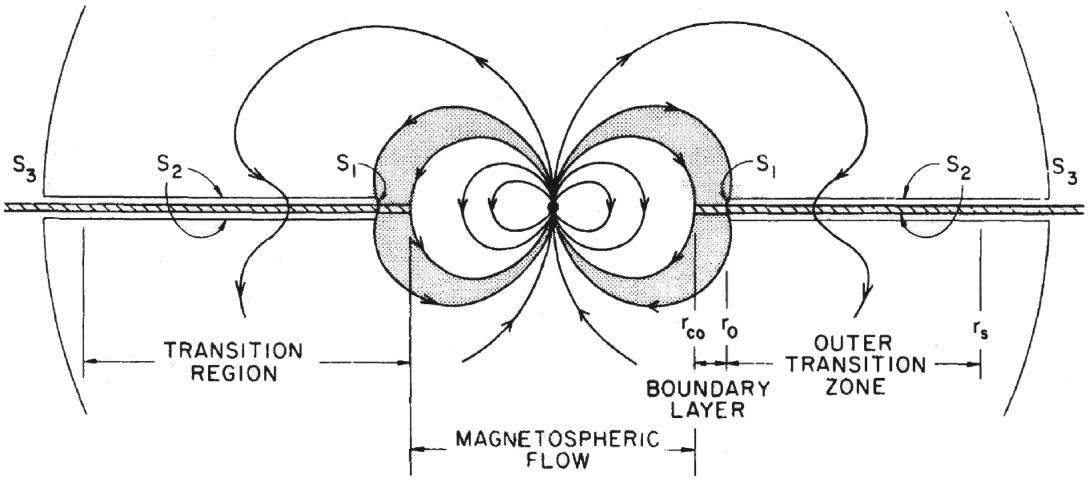

Figure 19. Side view of accretion flow from Ghosh & Lamb (1979).

If the pulse period is long, plasma is able to penetrate into the magnetosphere and reach the neutron star surface, transferring angular momentum and causing a strong spin-up torque. If the pulse period is short, the plasma is unable to penetrate further and the neutron star spins down.

The magnetic moment (μ) can be found if $\dot{P}$, P and L are known by assuming a given mass and radius and seeing which value of μ predicts the observed $\dot{P}$ using

$$-\dot{P} = 5.0 \times 10^{-5} \mu_{30}^{2/7} n(\omega_s) S_1(M) \left(P L_{37}^{3/7}\right)^2, \quad (2)$$

where μ_{30} is the magnetic moment in units of 10^{30} G cm^{-3} and L_{37} is the luminosity of the accreting star in units of 10^{37} erg s^{-1}. For an $0 < \omega_s < 0.9$

$$n(\omega_s) = 1.4(1 - 2.86\omega_s)(1 - \omega_s)^{-1} \quad (3)$$

within 5 per cent accuracy and

$$\omega_s = 1.35 \mu_{30}^{6/7} S_2(M) \left(P L_{37}^{3/7}\right)^{-1}$$

$$= 1.19 P^{-1} \dot{M}_{17}^{-3/7} \mu_{30}^{6/7} \left(\frac{M}{\mathrm{M}_\odot}\right)^{-5/7}, \quad (4)$$

where $\dot{M}_{17}$ is the mass accretion rate in units of 10^{17} g s^{-1} and $\frac{M}{\mathrm{M}_\odot}$ is assumed throughout to be 1.4. $S_1(M)$ and $S_2(M)$ are structure functions that depends on the mass equation of state and the dynamical response of the neutron star:

$$S_1(M) = R_6^{6/7} \left(\frac{M}{\mathrm{M}_\odot}\right)^{-3/7} I_{45}^{-1}, \quad (5)$$

where R_6 is the radius of the accreting star in units of 10^6 cm, assumed throughout to be 1, and I_{45} is the moment of inertia in units of 10^{45} g cm^2, and

$$S_2(M) = R_6^{-3/7} \left(\frac{M}{\mathrm{M}_\odot}\right)^{-2/7}. \quad (6)$$

The value of the magnetic field can then be calculated using

$$B = \frac{\mu}{R^3}. \quad (7)$$

Since $n(\omega_s)$ depends only on ω_s and ω_s is inversely proportional to $PL_{37}{}^{3/7}$, the $\dot{P}$ for a star of a given mass and magnetic moment depends only on $(PL_{37}{}^{3/7})^{-1}$. Fig. 20 shows that Swift J045106.8−694803 is located in the same region as GX 1+4, SAX J2103.5+4545, 4U 2206+54 and SXP 1062 on a plot of $\log_{10}(\dot{P})$ against $\log_{10}(PL_{37}{}^{3/7})$.

GX 1+4 is part of a LMXB, it is a slow rotator with a period of about 121 s and has been observed to have spun-down by about 2.6 s yr^{-1} (Chakrabarty et al. 1997). SAX J2103.5+4545 is part of a HMXB system, it is also a slow rotator with a pulse period of 358.166 ± 0.0005 s and a luminosity of $(2.0 \pm 0.5) \times 10^{36}$ erg s^{-1}. It has also been known to spin up at a rate of 4.69 ± 0.09 s yr^{-1} (Sidoli et al. 2005). This means that it has a magnetic field of $(1.47 \pm^{0.08}_{0.09}) \times 10^{14}$ G. 4U 2206+54 (Reig, Torrejon & Blay 2012) and SXP 1062 (Turolla & Popov 2012) are also part of HMXB systems, both are known to be spinning down and both were recently identified as having extremely high magnetic fields.

Highly magnetized neutron stars may be formed if a very magnetic star conserves its magnetic field during the neutron stars formation or, if the neutron star is rotating fast enough to start a dynamo effect during the first ∼20 s of its life. This converts heat and rotational energy into magnetic energy and increases the magnetic field (Ferrario & Wickramasinghe 2006).

The first evidence for highly magnetized accreting neutron stars came from Pizzolato et al. (2008), who showed that the X-ray source 1E 161348−5055 may contain a neutron star with a surface magnetic field of ∼10^{15}G which is part of an LMXB. This was shortly followed by Bozzo, Falanga & Stella (2008), who argued that highly magnetized neutron stars may also exist in HMXB.

Our results show that the $\dot{P}$ measured between 2008 and 2011 implies a magnetic field of $(1.3 \pm 0.1) \times 10^{14}$ G, whilst that measured between 2011 and 2012 implies a magnetic field of $(6 \pm 1) \times 10^{13}$ G. The value calculated for the whole duration of observations is $(1.2 \pm 0.1) \times 10^{14}$ G. Taking into account the highest and lowest possible values of B measured between 2008 and 2011, and 2011 and 2012, this value becomes $(1.2 \pm^{0.2}_{0.7}) \times 10^{14}$ G. Parameters calculated using equations (1)– (7) are shown in Table 4.

All values are over the quantum critical value of 4.4×10^{13} G, which means that the physics must be described with quantum field theory rather than classical physics. Although Swift J045106.8−694803 is powered by accretion, rather than due to the decay and instabilities of its magnetic field, and hence cannot be referred to as a magnetar yet, it has the potential to become one.

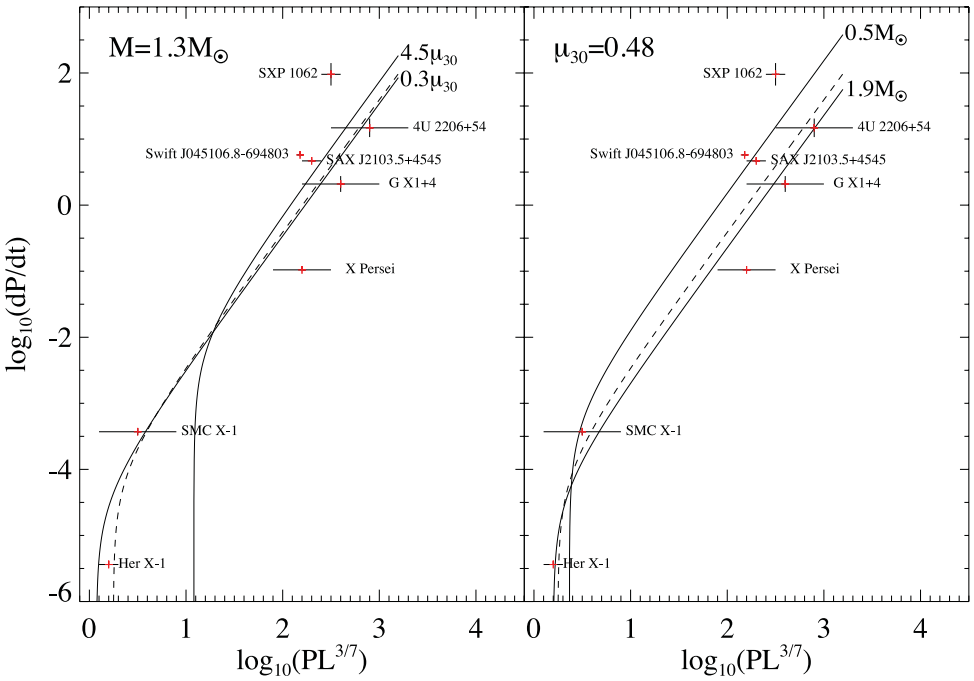

Figure 20. Logarithmic plot of $\dot{P}$ against $PL^{3/7}$ with contours calculated from Dachs, Hummel & Hanuschik (1992). Left-hand panel shows the theoretical curves for three values of stellar magnetic moment assuming a neutron star mass of 1.3 $M_{\odot}$. The dashed line shows the theoretical curve for $\mu_{30} = 0.48$. The right-hand panel shows the theoretical curves for three values of neutron star mass assuming a magnetic moment of $\mu_{30} = 0.48$. The dashed line is the theoretical curve for $M = 1.3\,M_{\odot}$. Data for Swift J045106.8−694803 and seven other pulsars are included in the plot. References are as follows: Her X-1 (Li, Dai & Wang 1995), SMC X-1 (Kahabka & Li 1999), X Per (Delgado-Martí et al. 2001), GX 1+4 (Ferrigno et al. 2007; Chakrabarty & Roche 1997), SAXJ2103.5+4545 (Sidoli et al. 2005), 4U 2206+54 (Reig et al. 2012) and SXP 1062 (Hénault-Brunet et al. 2012; Haberl et al. 2012).

Table 4. A summary of observed data and results derived using equations (1)– (7) for Swift J045106.8−694803.

Orbital period	21.631 ± 0.005 d
Pulse period in 2008 October /November	187.07 ± 0.04 s
Pulse period in 2011 October	169.8 ± 0.3 s
Pulse period in 2012 July	168.5 ± 0.2 s
Average luminosity	$(3.4 \pm 0.3) \times 10^{36}$ erg s^{-1}
$\dot{P}$	-5.01 ± 0.06 s yr^{-1} $(-1.59 \pm 0.02) \times 10^{-7}$ s s^{-1}
T_s	-34.9 ± 0.4 yr
$\log_{10}(\dot{P})$	0.70 ± 0.01
$\log_{10}(PL_{37}{}^{3/7})$	2.04 ± 0.04
ω_s	$0.7\pm^{0.1}_{0.3}$
$n(\omega_s)$	$-3\pm^{2}_{1}$
μ	$(1.2\pm^{0.2}_{0.7}) \times 10^{32}$ G cm^{-3}
B	$(1.2\pm^{0.2}_{0.7}) \times 10^{14}$ G

The Galactic HMXB system containing LSI 61303 recently showed magnetar-like behaviour when it underwent two bursts similar to those of soft gamma repeaters (SGRs) (Torres et al. 2012; Papitto, Torres & Rea 2012).

In conclusion, the spin-up rate of Swift J045106.8−694803 can be explained using Ghosh & Lamb (1979) accretion theory provided that it has a magnetic field of $(1.2\pm^{0.2}_{0.7}) \times 10^{14}$ G.

ACKNOWLEDGMENTS

We acknowledge the use of public data from the *Swift* and *RXTE* data archive and are grateful for the advice from Gerry Skinner on the *Swift*/BAT data. This paper utilizes public domain data obtained by the MACHO Project, jointly funded by the US Department of Energy through the University of California, Lawrence Livermore National Laboratory under contract No. W-7405-Eng-48, by the National Science Foundation through the Center for Particle Astrophysics of the University of California under cooperative agreement AST-8809616, and by the Mount Stromlo and Siding Spring Observatory, part of the Australian National University. The OGLE project has received funding from the European Research Council under the European Community's Seventh Framework Programme (FP7/2007–2013)/ERC grant agreement no. 246678 to AU. Optical observations were also made with ESO Telescopes at the La Silla Paranal Observatory under programme ID [088.D-0352(A)] and the SAAO 1.9 m telescope in South Africa. We also thank STFC whose studentships funded HK and ESB.

REFERENCES

Beardmore A. P., Coe M. J., Markwadt C., Osborne J. P., Baumgartner W. H., Tueller J., Gehrels N., 2009, Astron. Telegram, #1901
Bird A. J., Coe M. J., McBride V. A., Udalski A., 2012, MNRAS, 423, 3663
Bonanos A. Z., Castro N., Macri L. M., Kudritzki R.-P., 2011, ApJ, 729, L9
Borkowski K. J., Hendrick S. P., Reynolds S. P., 2006, ApJ, 652, 1259
Bozzo E., Falanga M., Stella L., 2008, ApJ, 683, 1031
Chakrabarty D., Roche P., 1997, ApJ, 489, 254
Chakrabarty D. et al., 1997, ApJ, 481, L101
Coleiro A., Chaty S., 2011, in Schmidtobreick L., Schreiber M., Tappert C., eds, ASP Conf. Ser. Vol. 447, Evolution of Compact Binaries. Astron. Soc. Pac., San Francisco, p. 265
Dachs J., Hummel W., Hanuschik R. W., 1992, A&AS, 95, 437
Delgado-Martí H., Levine A. M., Pfahl E., Rappaport S. A., 2001, ApJ, 546, 455

Dickey J. M., Lockman F. J., 1990, ARA&A, 28, 215
Evans C. J., Howarth I. D., Irwin M. J., Burnley A. W., Harries T. J., 2004, MNRAS, 353, 601
Evans C. J., Lennon D. J., Smartt S. J., Trundle C., 2007, A&A, 464, 289
Ferrario L., Wickramasinghe D., 2006, MNRAS, 367, 1323
Ferrigno C., Segreto A., Santangelo A., Wilms J., Kreykenbohm I., Denis M., Staubert R., 2007, A&A, 462, 995
Gardiner L. T., Noguchi M., 1996, MNRAS, 278, 191
Ghosh P., Lamb F. K., 1979, ApJ, 234, 296
Grebenev S. A., Lutovinov A. A., Tsygankov S. S., Mereminskiy I. A., 2012, preprint (arXiv:1207.1750v1)
Grimm H. J., Gilfanov M., Sunyaev R., 2003, MNRAS, 339, 793
Güver T., Özel F., 2009, MNRAS, 400, 2050
Haberl F., Sturm R., Filipović M. D., Pietsch W., Crawford E. J., 2012, A&A, 537, 1
Hénault-Brunet V. et al., 2012, MNRAS, 420, L13
Kahabka P., Li X.-D., 1999, A&A, 345, 117
Lennon D. J., 1997, A&A, 317, 871
Li X.-D., Dai Z.-G., Wang Z.-R., 1995, A&A, 303, L1
Liu Q. Z., van Paradijs J., van den Hauvel E. P. J., 2005, A&A, 442, 1135
Massey P., 2002, ApJS, 141, 81
McBride V. A., Bird A. J., Coe M. J., Townsend L. J., Corbet R. H. D., Haberl F., 2010, MNRAS, 403, 709
Morgan W. W., Keenan P. C., Kellman E., 1943, An Atlas of Stellar Spectra: With an Outline of Spectral Classification. The University of Chicago Press, Chicago, IL
Negueruela I., Coe M. J., 2002, A&A, 385, 517
Papitto A., Torres D. F., Rea N., 2012, ApJ, 756, 188
Paturel G., Dubois P., Petit C., Woelfel F., 2002, Comparison LEDA/SIMBAD October 2002. Catalogue to be published in 2003. LEDA, 0 (2002) 1 (2002): 0
Pizzolato F., Colpi M., De Luca A., Mereghetti S., Tiengo A., 2008, ApJ, 681, 530
Reig P., 2011, Ap&SS, 332, 1
Reig P., Torrejon J. M., Blay P., 2012, MNRAS, 425, 595
Sidoli L. et al., 2005, A&A, 440, 1033
Sturm R. et al., 2012, A&A, 542, A109
Torres D. F., Rea N., Esposito P., Li J., Chen Y., Zhang S., 2012, ApJ, 744, 106
Turolla R., Popov S. B., 2012, MNRAS, 421, L127
Walborn N. R., Fitzpatrick E. L., 1990, PASP, 102, 379
Wegner W., 2006, MNRAS, 371, 185
Wilms J., Allen A., McCray R., 2000, ApJ, 542, 914
Zaritsky D., Harris J., Thompson I. B., Grebel E. K., 2004, ApJ, 128, 1606

This paper has been typeset from a TEX/LATEX file prepared by the author.